Angle Measurement with a Phase Monopulse Radar Altimeter

J. Robert Jensen, *Member, IEEE*

***Abstract*— It is possible to enhance the conventional satellite radar altimeter in such a way that the range measurement is accompanied by an angle measurement. This is useful if the applications of these altimeters are to be expanded to include nonlevel surfaces such as continental ice sheets and land. The angle measurement can be made in one or two directions through the inclusion of one or two additional antennas and receiver channels and the integration of complex "cross-channel" waveforms whose phase indicates the angle to the point of first reflection from the scattering surface. This paper develops the measurement concept and establishes the precision of the resulting elevation measurement through an analysis of the dominant sources of error within the instrument. It is shown through analysis and numerical simulation that elevation errors over a flat tilted diffusely scattering surface can be maintained below the 1-cm level. The impact of antenna pointing and surface roughness are considered.**

***Index Terms*— Electromagnetic scattering inverse problems, monopulse radar, satellite altimiters.**

I. Introduction

ALL SATELLITE altimeters measure range by transmitting a pulse that is reflected by the Earth surface back to a receiver. The round-trip propagation time for the pulse is converted to range. The precise measurement of range from a profile of reflected power varies with each instrument. Following conventional radar altimeter terminology, this profile will be referred to in this paper as the altimeter "waveform." The characteristics of this waveform in ocean applications are well described in the literature [1], [2].

Satellite radar altimeters such as Topex are "pulse limited" in the sense that the radiated phase front meets the scattering surface over an area that is limited by the (compressed) width of the transmitted pulse. Laser altimeters, by contrast, are "beam limited" in that this area is limited by the transmit/receive beamwidth of the system. This results in quite different responses of these two systems to scattering surfaces that have a mean slope. The geometry of pulse-limited and beam-limited altimeter systems over level and tilted surfaces is shown in Fig. 1.

As shown in Fig. 1, surface tilt causes the measurement area for the pulse-limited altimeter to move away from the nadir point because the measurement area is always centered around the point on the scattering surface that is nearest to the altimeter. The waveform is the same for the level and tilted surfaces except for the effects of antenna weighting so long as the point of first reflection remains within the illuminated area. These antenna effects are absent to first order in the surface slope and become significant only as the slope approaches half of the radar beamwidth. The Topex beamwidth of about 1.2° is typical for a pulse-limited radar altimeter.

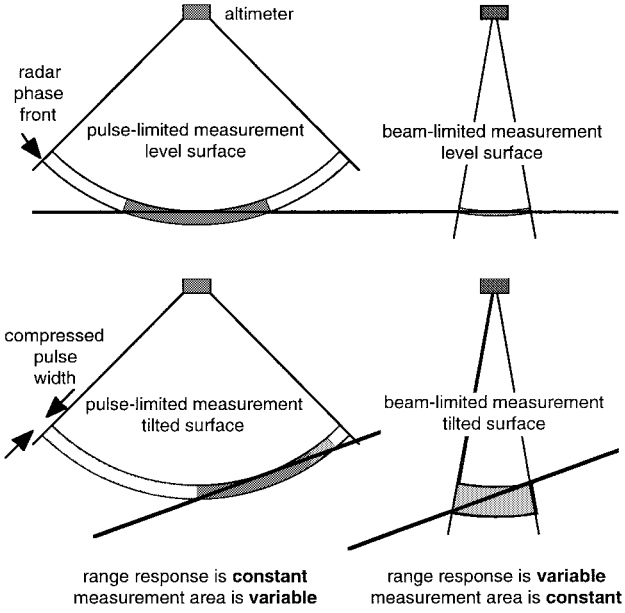

Fig. 1. Measurement response for pulse-limited and beam-limited altimeters over level and tilted surfaces. Surface tilt moves the measurement area but not the measurement response for a pulse-limited instrument. For a beam-limited instrument, however, the measurement area is unaffected but the response is broadened.

While the shape of the waveform is not altered for small surface slopes, the range measurement is directly affected. For a satellite altitude of 800 km, a surface slope of 0.1° results in the distance to the nearest point on the surface being 1.2 m less than the distance to the nadir point. Without information about the surface slope, the measured range is interpreted as being the distance to the nadir point and so a 1.2 m error is incurred. By comparison, we would like to have an elevation measurement accuracy below 10 cm in order to support long term ice sheet monitoring since this is the level of observed and expected changes [3] (see also, the discussion in [4] and [5]).

While some of the slope induced errors can be removed through a process of estimating the surface slope and computing corrections ([6] and [7], for example), this slope sensitivity has resulted in attention being turned away from the use

Manuscript received April 8, 1997; revised November 25, 1997.

The author is with the Applied Physics Laboratory, Johns Hopkins University, Laurel, MD 20723 USA.

Publisher Item Identifier S 0018-926X(99)04780-8.

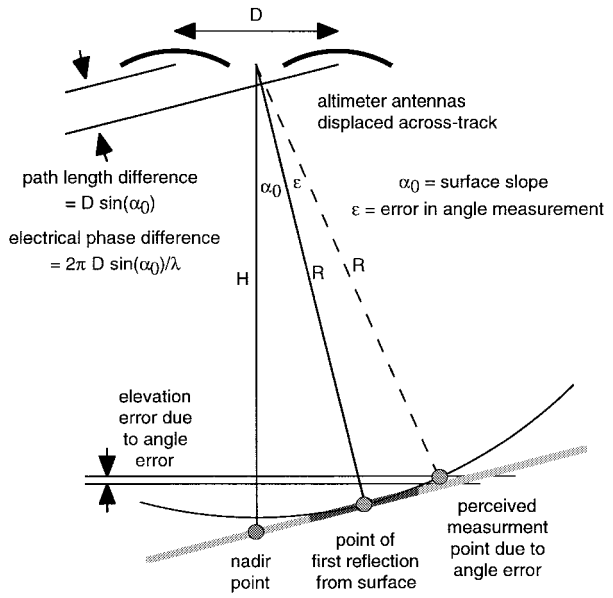

Fig. 2. Illustration of the phase comparison monopulse angle measurement. Without an angle measurement, the range is taken to be that of the subsatellite point. The angle measurement determines the horizontal and vertical position of the surface at the measurement point. It should be noted that the error is defined as the difference between the elevation of the inferred measurement point and the elevation of the surface at the horizontal position of the inferred measurement point.

of radar altimeters for applications such as measuring the continental ice mass balance and toward alternatives such as the GLAS laser altimeter [8]. Abandonment of radar for such applications results in the loss of some inherent strengths of radar systems. These include the ability to operate in the presence of cloud cover, which is significant in polar regions, and the ability to include a statistically significant, large area of the surface within each range measurement.

This paper will establish that the addition of an angle measurement capability to a conventional satellite radar altimeter is practical and that it results in high-precision elevation measurements over tilting surfaces. The angle measurement is accomplished through the addition of a receive-only antenna and a second receiver channel to a radar altimeter. A phase difference between the backscattered pulse at the two antennas indicates the angle of the scattering as shown in Fig. 2. The details of implementing this angle measurement and the statistical performance of the resulting system are presented in subsequent sections of this paper. While only a single angle measurement will be considered here, it is possible to generalize the results to the measurement of two angles in perpendicular planes.

It is expected that the most useful implementation of the angle measurement described here will be in conjunction with another altimeter enhancement referred to as the "delay/Doppler" altimeter [9]. This concept is described in a companion paper [10]. Together, this allows for a control of the measurement area position in the along-track direction through the use the delay/Doppler technique and a determination of the measurement area position in the across-track direction through the angle measurement. These techniques complement each other by working at right angles. The angle measurement may be employed alone, however, to produce a determination of the measurement area position in two dimensions.

II. Instrument Analysis

A. Height Error Definition

The ultimate goal of the altimeter angle measurement is an elevation determination. Angle errors will result in elevation errors. The proper definition of the elevation error must account for the pulse-limited nature of the radar altimeter range measurement. The range and angle combine to produce both a horizontal and a vertical position of the point of first reflection on the scattering surface as shown in Fig. 2. An angle error will affect both components of the position. The elevation error is defined in this paper as the difference between the measured elevation and the elevation of the true surface at the measured horizontal position.

At the small incidence angles of interest here, range errors will translate directly into elevation errors and so range errors will be an additive error source. Errors in the range measurement will be ignored in this section while we focus on angle errors.

The altimeter will be located at a height H above a surface with slope α_0. The actual range and angle to the point-of-first-reflection on the scattering surface are (R, α_0), where

$$R = H\cos(\alpha_0). \tag{1}$$

The measured range and angle are $(R, \alpha_0+\varepsilon)$ where ε is the angle measurement error. The horizontal and vertical positions inferred from the measurements are

$$x = R\sin(\alpha_0+\varepsilon) = H\cos(\alpha_0)\sin(\alpha_0+\varepsilon) \tag{2}$$

$$z = -R\cos(\alpha_0+\varepsilon) = -H\cos(\alpha_0)\cos(\alpha_0+\varepsilon) \tag{3}$$

where the vertical position is measured relative to the altimeter position. The angle error ε may be due to a combination of spacecraft attitude knowledge errors and instrument measurement errors.

The vertical position of the scattering surface at position x is

$$\tilde{z} = -H + x\tan(\alpha_0) \tag{4}$$

and the elevation error is

$$z - \tilde{z} = H[1-\cos(\varepsilon)] \approx \frac{H\varepsilon^2}{2}. \tag{5}$$

It is quite significant that the elevation error is without a linear dependence on the angle error and without a dependence on the surface slope. This follows from the pulse-limited nature of the measurement. By contrast, a beam-limited instrument pointed nominally at nadir will produce a measured range of

$$R_{beam} = \frac{H}{\cos(\varepsilon)+\sin(\varepsilon)\tan(\alpha_0)} \tag{6}$$

and the elevation error is

$$R_{beam} - H = \frac{H}{\cos(\varepsilon)+\sin(\varepsilon)\tan(\alpha_0)} - H \approx \frac{H\varepsilon^2}{2}(1+2\tan^2(\alpha_0)) - H\varepsilon\tan(\alpha_0). \tag{7}$$

When the surface slope is zero, there is no distinction between the pulse-limited and beam-limited elevation error expressions. However, if slope is present, then the impact of an attitude error, for example, will be quite different for the two instruments. If we consider an altitude of 800 km, a surface slope of 0.5°, and an attitude error of 0.01° (175 μrad), the pulse-limited elevation error is 1.22 cm while the beam-limited elevation error is two orders of magnitude larger at 1.22 m.

A pulse-limited system will combine the errors due to attitude determination with errors due to the backscatter angle measurement. Only the attitude errors are present in a beam-limited system. However, as we see in this example, the pulse-limited instrument has reduced attitude knowledge requirements and lacks a strong attitude control requirement. We can also see that the total angle noise must be at the 0.01° level in order to support centimeter scale elevation precision. Such precision is possible with a reasonable radar altimeter, as will be demonstrated below.

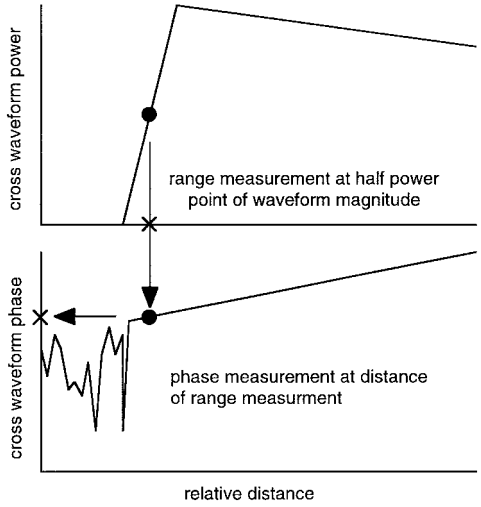

Fig. 3. Illustration of the process of determining range and angle from the direct and cross-channel altimeter waveforms. The waveform magnitude establishes the point at which the waveform phase is extracted to determine the measurement geometry.

B. Angle Measurement Procedure

The procedure for making an angle measurement within a radar altimeter follows the same lines as the signal processing within a conventional instrument such as Topex [11]. All of the processing of the reflected signal in a conventional altimeter is duplicated in a second receiving channel through the Fourier transform that converts frequency offsets to range offsets. At this point in a conventional system, the phase of the transform is thrown away and only the power within each range bin is of interest. These square-magnitude values are integrated over many pulses to reduce the coherent speckle (or Rayleigh fading) noise. Prior to averaging, each range bin has a power that is distributed as a chi-square variate with two degrees of freedom. Averaging increases the number of degrees of freedom and the total improvement depends on the independence of successive pulses.

Within an angle measuring altimeter, this procedure is followed for one (or both) of the receiving channels, but in addition, a complex cross-channel waveform is produced by multiplying the transform output of one channel, range bin by range bin, and the complex conjugate of the transform output of the other channel. The phase of each value in this cross-channel waveform indicates the phase difference of the backscattered pulse at the two antennas. These cross-channel waveforms are integrated over many pulses as before, with the only difference being that we are integrating complex rather than real values.

The angle is determined from the integrated waveform by its phase at the surface range. The range to the scattering surface is determined through processing either the direct-channel or the cross-channel waveform in the conventional sense (e.g., gate tracking for Topex [11]). After this range has been determined, the phase of the cross-channel waveform at this range is found. Averaging of several waveform samples prior to angle measurement will be useful to some extent and will improve the angle measurement precision.

Fig. 3 shows idealized waveform power and phase for cross waveforms. Receiver noise dominates prior to the waveform leading edge, so the phase of the cross-channel waveform there will be meaningless. At the leading edge, the phase will have the most stability as will be shown below.

The phase of the cross-channel waveform is determined by the path length difference between the two antennas and the point of first reflection on the scattering surface. The mean value of the cross-channel waveform phase (in radians) is

$$\theta = kD\,\sin(\alpha) \approx kD\alpha \tag{8}$$

where k is the radar wavenumber ($=2\pi/\lambda$), D is the separation of the antenna phase centers, and α is the angle between the reflecting point and a line normal to the antenna separation.

Throughout this paper, the quantities of interest will be illustrated with the example parameters shown in Table I. Here we consider a Ku-band radar (2.2-cm wavelength) with a separation of 0.6 m, the relationship between the measured phase and the geometric angle is

$$\theta = 171.36\alpha. \tag{9}$$

Combined with our determination above that angle measurement precision on the order of 0.01° will be required in order to support elevation precision on the order of 1 cm, we see here that phase measurement precision must be on the order of 1.4°. This is a strict requirement, but it is practical given the amount of integration available to either a conventional or a delay/Doppler radar altimeter. (The amount of available integration for the delay/Doppler radar can be larger than for the conventional altimeter in spite of the coherent processing because of the higher allowed pulse repetition rates and because integration is performed over the entire time that a measurement area is within the antenna beamwidth [10].)

We can also see here that an unambiguous angle measurement can be made only over an interval of about 2.5°. This is sufficient for almost all of the continental ice sheets. If larger angle ranges are required, then a means of grating lobe resolution must be included. This may be achieved by displacing the boresights of the two antennas and comparing

TABLE I
PARAMETERS USED THROUGHOUT THE PAPER TO ILLUSTRATE THE PERFORMANCE OF ANGLE MEASUREMENT STATISTICS

parameter	variable	value
radar wavelength	λ	0.022 m
aperture displacement	D	0.6 m
satellite altitude	H	800 km
antenna beamwidth	-	1.5°
range resolution	Δ	0.47
amount of integration	N	100 waveforms

powers in the two receiving channels as was done within the MSX Beacon Receiver [12].

C. Elevation Measurement Statistics

The standard deviation of the elevation error, given the above definition of the error in (5), is related to the statistics of the angle measurement as

$$\text{rms}\{z-\tilde{z}\} = \frac{H}{2}\sqrt{E\{(\alpha-\alpha_0)^4\}} \tag{10}$$

where $E\{\ \}$ is the mean value of the enclosed quantity, α is the measured angle, and α_0 is the mean value of this angle. The mean angle will be equal to the surface slope.

In order to compute the standard deviation of the elevation, we therefore need the fourth moment of the measured angle. The statistics of this angle will be determined from an exact statistical analysis and also from an approximate expression developed in the next section.

D. Angle Measurement Statistics

Noise will be present in the angle measurement because the signals present in the two receiver channels are not perfectly correlated. Thermal receiver noise is one source of statistical independence in the two channels. Uncorrelated speckle noise is another. The surface reflection results from the coherent summation of scattering from many individual, small scattering areas. Because the antenna phase centers are separated, these contributions have different relative phases in the two viewing geometries and this leads to some loss of coherence between the two signals. In this section, we will relate the angle measurement requirements to a requirement for coherence between the two receiver channels.

We will assume throughout this discussion that the waveform values are jointly Gaussian. This is expected for both the surface scattered portion and the thermal noise portion because of the impact of the central limit theorem acting upon the many individual contributions to these values.

We will denote a waveform value from one channel as v_+ and the corresponding waveform value from the other channel as v_-. These are the complex values that result from the Fourier transform of the deramped signal, prior to computation of the square magnitude for integration in a conventional altimeter [11]. Where a quantity is independent of the channel, the subscript is omitted.

The joint probability density function for the complex values v_+ and v_- under the jointly Gaussian assumption is

$$p(v_+, v_-) = \frac{1}{(2\pi)^2|\underline{\underline{D}}|}\exp\left\{-\frac{1}{2}\begin{pmatrix}v_+\\ v_-\end{pmatrix}^t \underline{\underline{D}}^{-1}\begin{pmatrix}v_+\\ v_-\end{pmatrix}\right\} \tag{11}$$

where

$$\underline{\underline{D}} = \frac{1}{2}E\left\{\begin{pmatrix}v_+v_+^* & v_-v_+^*\\ v_+v_-^* & v_-v_-^*\end{pmatrix}\right\} = \frac{E\{|v|^2\}}{2}\begin{pmatrix}1 & \eta\\ \eta & 1\end{pmatrix} \tag{12}$$

and

$$\eta = E\{v_+v_-^*\}/E\{|v|^2\}. \tag{13}$$

We will assume here that the mean of the angle measurement is zero and so η is real. This simplifies the expressions by eliminating a mean term in the measured angle, but it results in no loss of generality in the discussion of the statistics of the measurement.

The cross-channel product waveform sample is γ, defined as

$$\gamma = v_+v_-^*. \tag{14}$$

Equation (11) may converted to a probability density function for γ as

$$p_1(\gamma) = \frac{2/E\{|v|^2\}}{\pi(1-\eta^2)}K_0\left(\frac{2|\gamma|/E\{|v|^2\}}{1-\eta^2}\right) \times \exp\left\{\frac{2\eta\Re\{\gamma\}/E\{|v|^2\}}{1-\eta^2}\right\} \tag{15}$$

where $\Re\{\gamma\}$ is the real part of γ. $K_0(\ )$ is the modified Bessel function [13].

If γ_N results from the sum of N independent products of v_+v_-, then we have the result

$$p_N(\gamma_N) = \frac{2|\gamma_N|^{N-1}/E^N\{|v|^2\}}{(N-1)!\pi(1-\eta^2)}K_{N-1}\left(\frac{2|\gamma_N|/E\{|v|^2\}}{1-\eta^2}\right) \times \exp\left\{\frac{2\eta\Re\{\gamma_N\}/E\{|v|^2\}}{1-\eta^2}\right\}. \tag{16}$$

We are interested only in the phase of γ_N for the angle measurement. The distribution of phase for $N=1$ is developed in [14]. The probability density function for the general cuase can be found to be

$$p_N(\theta) = \frac{1}{\pi(N-1)!}\left(\frac{1-\eta^2}{2(1-\xi^2)}\right)^N \times \left[f_{N-1}(\xi^2) + \frac{\xi(2N-1)!!}{\sqrt{1-\xi^2}}\cos^{-1}(-\xi)\right] \tag{17}$$

where

$$\xi = \eta\cos\theta$$

and

$$(2N-1)!! = (2N-1)(2N-3)(2N-5)\cdots 1.$$

The function $f_m(z)$ is defined by the recursion relation

$$f_0(z) = 1 \tag{18a}$$

$$f_m(z) = z(2m-1)!! + 2mf_{m-1}(z) + 2z(1-z)\frac{d}{dz}f_{m-1}(z). \tag{18b}$$

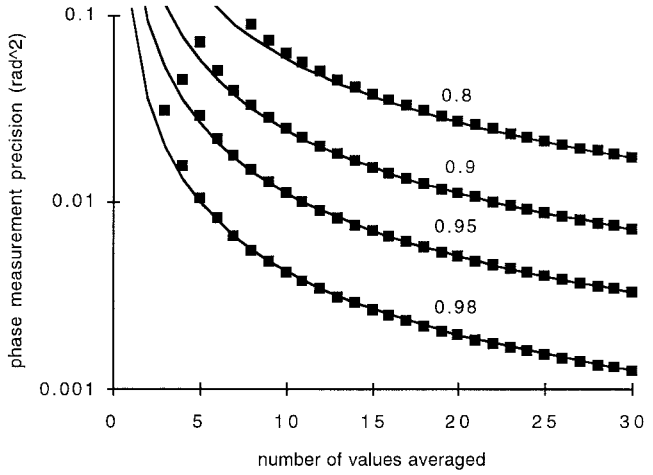

Fig. 4. Comparison of the exact and approximate expressions for the angle measurement precision as a function of the amount of integration performed for coherence values of 0.8, 0.9, 0.95, and 0.99. The square symbols are the result of numerically integrating (17). The curves are the approximation in (19).

The first few functions in this series are

$$f_1(z) = 2 + z \tag{18c}$$

$$f_2(z) = 8 + 9z - 2z^2 \tag{18d}$$

$$f_3(z) = 48 + 87z - 38z^2 + 8z^3. \tag{18e}$$

These equations may be used to compute the phase angle precision based on the cross-channel coherence η. They are a bit cumbersome, however, since they require the use of a recursion relation and numerical integration of the density function to determine the standard deviation of the angle. The fourth moment of the measured angle is approximately

$$\sqrt{E\{\theta^4\}} \approx \frac{\sqrt{3}(1/\eta^2 - 1)}{2N} \times \left(1 + \frac{2}{N}\right). \tag{19}$$

This approximate expression for the variance of θ^2 is compared with the value determined from the probability density function in (17). The results from both approaches are shown in Fig. 4 for the cases of $\eta = 0.8$, 0.9, 0.95, and 0.99, and N ranging from 1 to 30. It is seen that (19) is a good approximation when several waveforms are integrated. For large N, the final factor in 919) can be neglected.

Combining (19) with (8) and (10) above, we have

$$\begin{aligned} \text{rms}\{z - \tilde{z}\} &= \frac{H}{2}\sqrt{E\{\alpha^4\}} \\ &= \frac{H}{2(kD)^2}\sqrt{E\{\theta^4\}} \\ &= \frac{\sqrt{3}H(1/\eta^2 - 1)}{4(kD)^2 N}. \end{aligned} \tag{20}$$

We are interested in an elevation precision on the order of 1 cm. Using the values shown in Table I, the cross-channel coherence required to achieve this performance is 0.96 when 100 waveforms are integrated. For reference, the Topex altimeter integrates 228 waveforms prior to any analysis by the signal processor [11]. It will be shown later that this coherence places a lower limit of 13.8 dB on the single waveform sample signal-to noise ration (SNR).

E. Cross-Channel Phase Coherence

The coherence of the two receiver channels can be obtained by first breaking the signal into a surface scattered term and a receiver noise term as

$$v_\pm = s_\pm + n_\pm. \tag{21}$$

The $\pm$ indicates the direction of displacement of the antenna center from the antenna midpoint. The terms s_+ and s_- are correlated with each other but are independent of the noise terms, as the noise terms are of each other.

The signal coherence can be rewritten as

$$\eta = \frac{E\{v_+ v_-^*\}}{E\{|v|^2\}} = \frac{E\{s_+ s_-^*\}}{E\{|s|^2\} + E\{|n|^2\}} = \eta_S \eta_N \tag{22}$$

where

$$\eta_S = \frac{E\{s_+ s_-^*\}}{E\{|s|^2\}} \tag{23}$$

and

$$\eta_N = \frac{1}{1 + E\{|n|^2\}/E\{|s|^2\}}. \tag{24}$$

In order to compute the scattered signal coherence in (23), we will consider two cases. The first is relevant to the application of angle measurement within an otherwise conventional altimeter in which the measurement footprint is an annular area on the scattering surface [2]. The second is relevant to a Delay/Doppler altimeter in which the measurement footprint is narrowed in the along-track direction through the application of coherent processing. Such an altimeter is described in a companion paper [10]. For the present purpose, we will take for granted that such an instrument produces a narrow measurement area. For both cases, we will assume that the reflection coefficient $\rho(r)$ of the scattering surface is spatially white.

For any pulse-limited altimeter, the measurement area for the nth altimeter range gate will have a maximum and minimum distance given by

$$\max_n = \sqrt{[H + n\Delta]^2 - H^2} \approx \sqrt{2nH\Delta} \tag{25a}$$

and

$$\begin{aligned} \min_n &= \sqrt{[H + (n-1)\Delta]^2 - H^2} \\ &\approx \sqrt{2(n-1)H\Delta} \end{aligned} \tag{25b}$$

where the indexing of range gates is done such that $n = 1$ corresponds to a gate whose minimum distance just includes the scattering surface. The geometry leading to these distances is shown in Fig. 5. These ranges will be used below to quantify the signal coherence.

F. Scattered Signal Coherence Case 1—Annular Measurement Area

The surface scattered term can be written as

$$\begin{aligned} s_\pm = \int_{r_1}^{r_2} dr \int_0^{2\pi} d\theta r \rho(r, \theta) \\ \times \exp\left\{ik\sqrt{H^2 + (r\cos\theta \pm D/2)^2 + (r\sin\theta)^2}\right\} \end{aligned} \tag{26}$$

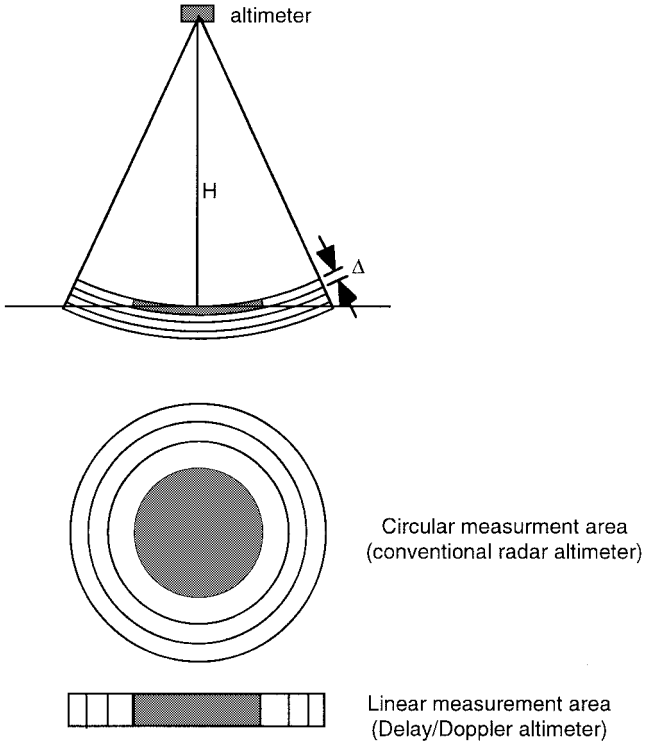

Fig. 5. Altimeter range gates for both annular and linear measurement areas.

where r_1 and r_2 are the inner and outer radii of the measurement annulus as defined by (25). Equation (26) can be approximated as

$$s_{\pm} \approx \int_{r_1}^{r_2} dr \int_0^{2\pi} d\theta r \tilde{\rho}(r, \theta) \exp\{ik(r^2 \pm Dr \cos\theta)/2H\} \tag{27}$$

where

$$\tilde{\rho}(r, \theta) = \rho(r, \theta) \exp\{ikH\}. \tag{28}$$

The approximation behind (27) will be very good since $D \ll r \ll H$. H will be hundreds of kilometers, r will be on the order of kilometers, and the value of D will be less than one meter.

The backscatter from the surface will decorrelate in a distance that is small compared to size of the scattering area. Therefore, we will assert that

$$E\{\tilde{\rho}(r, \theta)\tilde{\rho}^*(r', \theta')\} = E\{\rho(r, \theta)\rho^*(r', \theta')\}$$

$$= \sigma\delta(r - r')\delta(\theta - \theta')/r. \tag{29}$$

The scattered signal part of the cross-channel waveform is

$$s_+ s_-^* = \int_{r_1}^{r_2} dr \int_0^{2\pi} d\theta \int_{r_1}^{r_2} dr' \int_0^{2\pi} d\theta' r r' \tilde{\rho}(r, \theta)\tilde{\rho}^*(r', \theta') \times \exp\{ik[r^2 - r'^2 + D(r\cos\theta + r'\cos\theta')]/2H\}. \tag{30}$$

TABLE II
COMPUTED PHASE COHERENCE OF THE SURFACE SCATTERED SIGNAL FOR SEVERAL WAVEFORM RANGE GATES FOR BOTH ANNULAR AND LINEAR MEASUREMENT AREAS. A FLAT SCATTERING SURFACE IS ASSUMED

Inner distance (km)	Outer distance (km)	Annular area coherence	Linear area coherence
0	0.866	0.9957	0.9943
0.866	1.225	0.9871	0.9747
1.225	1.5	0.9785	0.9573
1.5	1.732	0.9699	0.9400

Combining the two equations above, it is easy to show that

$$E\{s_+ s_-^*\} = \sigma \int_{r_1}^{r_2} dr \int_0^{2\pi} d\theta r \exp\{ikDr\cos\theta/H\}$$
$$= 2\pi\sigma \int_{r_1}^{r_2} dr r J_0(kDr/H) \tag{31}$$

and

$$E\{|s|^2\} = \sigma \int_{r_1}^{r_2} dr \int_0^{2\pi} d\theta r = \pi\sigma(r_2^2 - r_1^2) \tag{32}$$

where $J_0(\ )$ is the Bessel function of the first kind [13]. The coherence of this scattered signal is then

$$\eta_S = \frac{E\{s_+ s_-^*\}}{E\{|s|^2\}}$$
$$= \frac{2}{(r_2^2 - r_1^2)} \int_{r_1}^{r_2} dr r J_0(kDr/H)$$
$$\approx 1 - (kD/H)^2(r_2^2 + r_1^2)/8 + (kD/H)^4(r_2^4 + r_2^2 r_1^2 + r_1^4)/192 \tag{33}$$

where the approximation has resulted from retaining the first three (constant, quadratic, and quartic) terms in the expansion of the Bessel function. This will be a good approximation so long as $(kDr/H)^2 \ll 1$. (This quantity has a value of 0.034 for the values shown in Table I and a measurement area radius of 866 m.)

For the parameters shown in Table I, the computed coherence of the scattered signal for the first range bin is 0.9957. For this bin, the inner radius is zero and the outer radius is 866 m. This coherence is well above the required coherence. As the range cells expand, the coherence will decrease rapidly. For a measurement area that consists of an annulus with an inner radius of 866 m and an outer radius of 1275 m, the coherence for the above parameters drops to 0.9871. For the next bin the coherence is 0.9785. These values are shown in Table II. The cross-channel coherence of the signal is sufficient in this case to support the 1 cm elevation precision requirement.

While no further approximations are necessary, it is interesting to further approximate (33) for the annular measurement area and derive an expression for the elevation accuracy. For high coherence values

$$1/\eta_S^2 - 1 \approx (kD/H)^2(r_1^2 + r_2^2)/4 = \frac{(kD)^2\Delta}{2H} \tag{34}$$

where only the terms through second order in r have been retained here and we have used the radii for the first waveform sample as given by (25). Substituting this into (20) yields

$$\text{rms}\{z-\tilde{z}\}=\frac{\sqrt{3}\Delta}{8N}. \tag{35}$$

It is noteworthy, and perhaps surprising, that this equation involves only the altimeter range resolution and the number of waveforms integrated. All other radar parameters have disappeared. In this approximation, the elevation precision is 0.1 cm, based on a range resolution of 0.47 m and 100 waveforms integrated. A more exact value of the elevation precision is obtained from (20) and (33), but for the first range bin and the parameters in Table I, the two expressions give nearly identical results.

It is also important that the elevation precision decreases as $1/N$. Increasing the amount of integration in the altimeter will proportionately improve the measurement precision.

G. Signal Coherence Case 2—Linear Measurement Area

For this case, we will consider a measurement area that has extent only in the direction parallel to the aperture displacement. The derivation procedure follows the same lines as that for the annular measurement area above.

For this case

$$s_{\pm}=\int_{x_1}^{x_2}dx[\rho(x)+\rho(-x)]\exp\left\{ik\sqrt{H^2+(x\pm D/2)^2}\right\} \tag{36}$$

where the measurement area consists of two intervals on either side of the nadir point as given by (25). Equation (36) is approximated as

$$s_{\pm}=\int_{x_1}^{x_2}dx[\tilde{\rho}(x)+\tilde{\rho}(-x)]\exp\{ik(x^2\pm xD)/2H\} \tag{37}$$

and the second moments are computed to be

$$\begin{aligned}E\{s_+s_-^*\}&=\sigma\int_{x_1}^{x_2}dx[\exp\{ikxD/H\}+\exp\{-ikxD/H\}]\\&=\frac{2\sigma H[\sin(kx_2D/H)-\sin(kx_1D/H)]}{kD}\end{aligned} \tag{38}$$

and

$$E\{|s|^2\}=2\sigma\int_{x_1}^{x_2}dx=2\sigma[x_2-x_1] \tag{39}$$

where we have again used the spatially white nature of the backscatter reflection coefficient. The coherence of the scattered signal is

$$\eta_S=\frac{E\{s_+s_-^*\}}{E\{|s|^2\}}=\frac{H[\sin(kx_2D/H)-\sin(kx_1D/H)]}{kD[x_2-x_1]}. \tag{40}$$

For a linear measurement area and the parameters considered above, the computed coherence is 0.9943 for the first range gate. This is still sufficient to support the required geometric angle measurement precision.

Equation (40) can be further approximated as

$$\eta_S\approx 1-\left(\frac{kD}{H}\right)^2(x_1^2+x_1x_2+x_2^2)/6. \tag{41}$$

Following the same lines as above for the annular measurement area, we can make a final simplification by assuming high coherence and make the approximation

$$1/\eta_S^2-1\approx\left(\frac{kD}{H}\right)^2(x_1^2+x_1x_2+x_2^2)/3=\frac{2(kD)^2\Delta}{3H} \tag{42}$$

for the first range sample using (25). The elevation precision becomes

$$\text{std}\{z-\tilde{z}\}=\frac{\Delta}{2\sqrt{3}N} \tag{43}$$

where as before, only the range resolution and the number of waveforms integrated appear in the final expression. For the linear measurement area case, the precision is poorer by a factor of 4/3 than for the annular measurement area case.

H. Thermal Receiver Noise Coherence

The coherence due to the thermal noise was given in (24) and may be expressed as

$$\eta_N=\frac{1}{1+1/\text{SNR}} \tag{44}$$

where SNR is the signal-to-noise ratio within the range bin being considered. Substituting this into (20), the elevation precision limit is

$$\text{rms}\{z-\tilde{z}\}=\frac{\sqrt{3}H(2/\text{SNR}+1/\text{SNR}^2)}{4(kD)^2N}. \tag{45}$$

Here we see that the elevation measurement precision depends on the altitude, the radar frequency, and the aperture displacement. We see from the above equation and the parameters in Table I that a SNR in excess of 13.8 dB will be required if a single, averaged waveform sample is to be used in the angle determination. The required SNR may be reduced by averaging samples, as will be demonstrated below.

III. Simulation Results

A computer simulation of the operation and statistics of a phase comparison angle measurement has been performed. The simulation is based on assigning a random reflectivity to each small area of a flat diffusely scattering surface and computing the contribution to the waveforms in each of the receiver channels. The surface may be level or tilted.

Fig. 6 shows the result of averaging 10 000 waveforms for the parameters given in Table I and a SNR of 10 dB. Fig. 6(a) contains the two direct-channel waveforms and the magnitude of the cross-channel waveform. The direct-channel waveforms exhibit a noise floor prior to the surface reflection range. The cross-channel waveform has no noise floor because the noise is independent in the two receiver channels. The magnitude in the cross-channel waveform is close to that of the direct-channel waveforms near the surface reflection, then falls away because of the reduced coherence as predicted by the analysis above. The shape of the cross-channel waveform is the product of that predicted by the Brown model [1] and the magnitude of the cross-channel coherence. The phase of the cross-channel

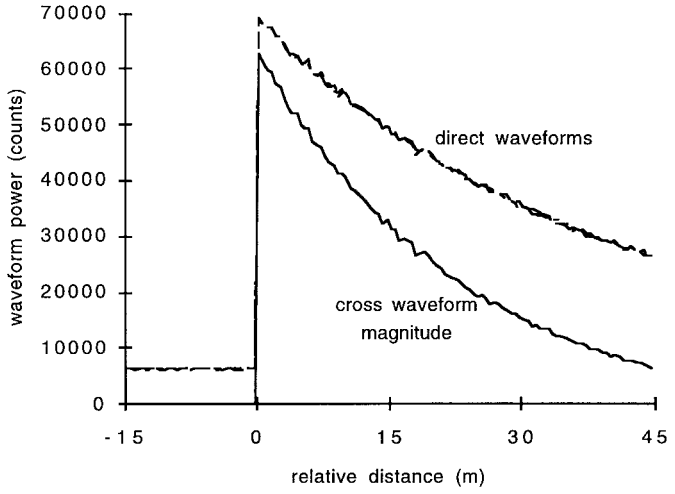

(a)

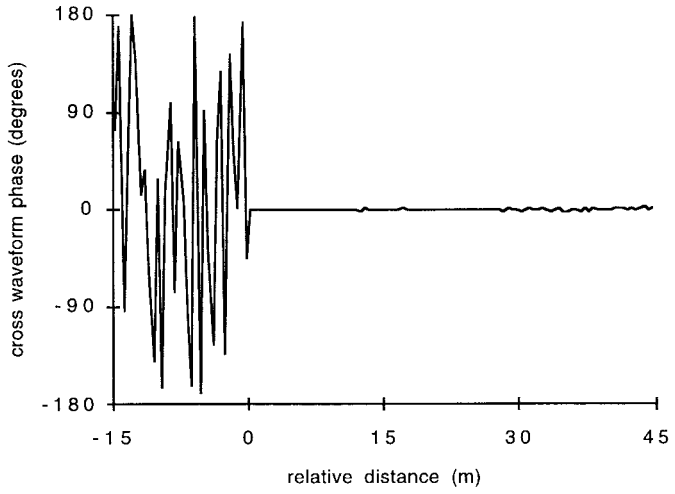

(b)

Fig. 6. Sum of 10 000 simulated direct and cross-channel waveforms for a 10 dB SNR. Other parameters are as shown in Table I. (a) The direct-channel waveforms and the magnitude of the cross-channel waveform. (b) The phase of the cross-channel waveform.

waveform is shown in Fig. 6(b). It is completely random prior to the surface reflection. Because so much averaging has been performed and the simulated scattering surface is level, the phase of the cross-channel waveform after the surface reflection stays very close to zero.

The coherence of the cross-channel waveform in Fig. 6 can be computed by taking the ratio of the cross-channel waveform magnitude and the magnitude of either of the direct-channel waveforms. The numerical results were found to be in excellent agreement with (33).

The statistics of the elevation measurement have been investigated by performing 1000 simulations that each involve the averaging of 100 waveforms. For a 10-dB SNR, the standard deviation of the simulated elevation is 2.56 cm while the predicted value is 2.60 cm based on (35). The results for SNR's of 10, 15, 20, 25, and 30 dB are shown in Fig. 7. In all cases, the simulated values are within 0.05 cm of the predicted values.

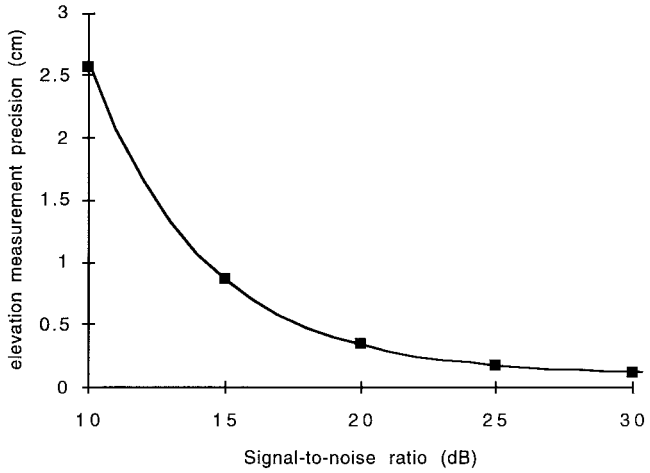

Fig. 7. Predicted and simulated precision of the elevation measurement for several values of the SNR. The curve is based on the equations in the paper. (Each simulated point is based on 1000 simulations, each resulting from 100 waveforms being averaged.) System parameters are as shown in Table I.

IV. Other Effects

A. Impact of the Antenna Beam Pattern

The results of the previous section pertain to an antenna baseline that is parallel to the scattering surface and antenna pointing that is normal to the this surface. The simulation used to produce the waveforms in Fig. 6 have been redone for a surface slope of 0.3°. The result is shown in Fig. 8. Two observations may be made about the phase plotted in Fig. 8(b). First, the phase is not zero at the point of surface reflection. The phase value at that point is the indicator of the scattering angle, as has been discussed above.

The second observation is that the phase has a slope. This slope results from the fact that the peak of the antenna gain remains at the subsatellite point, but the point of first reflection is away from that point, as was discussed in connection with Fig. 1. While the surface reflectivity has been assumed to be uniform, the antenna beam pattern will weight some areas more than others and produce a bias in the observed phase for points that are away from the waveform leading edge.

In order to eliminate the effects of this phase slope on the angle measurement, we will estimate both the phase at the track point and the phase slope. This can be done by minimizing an error term defined by

$$\varepsilon^2 = \sum_{n=n_1}^{n_2} \frac{\eta_n^3}{1-\eta_n} \sin^2(\phi_n - \theta - \beta n) \tag{46}$$

with respect to θ and β where ϕ_n is the phase of the nth point in the cross-channel waveform and η_n is the coherence of the nth point. This coherence is the ratio of the cross-channel waveform magnitude divided by the direct-channel waveform magnitude (or the geometric mean of both direct-channel magnitudes). The values of n_1 and n_2 are chosen to straddle the track point. Minimizing the error defined by (46) results in a maximum likelihood estimate of θ and β.

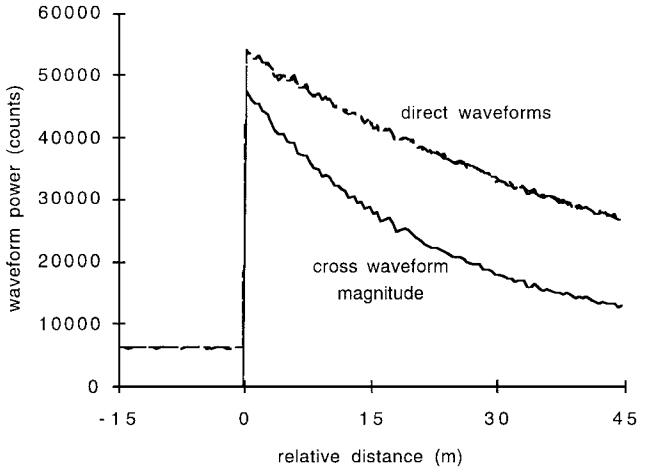

(a)

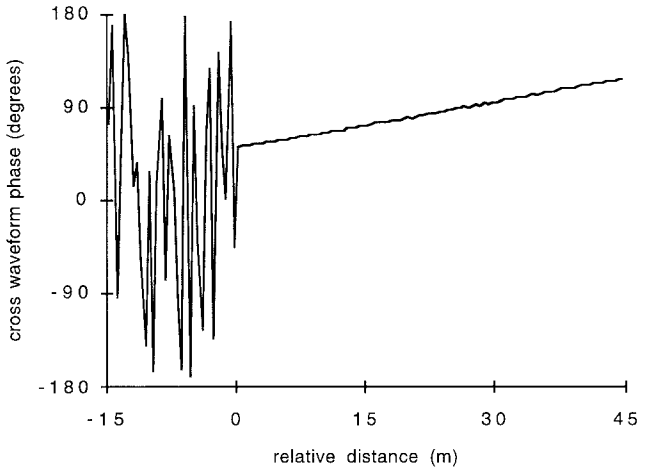

(b)

Fig. 8. Sum of 10 000 simulated direct and cross-channel waveforms for a 10-dB SNR and a 0.3° surface tilt. Other parameters are as shown in Table I. (a) The direct-channel waveforms and the magnitude of the cross waveform. (b) The phase of the cross-channel waveform.

The term preceding the sine function acts to give greater weight to waveform points with high coherence. Without the proper weighting, averaging of waveform points to estimate the scattering angle results in poorer performance, especially at low SNR's.

Once the minimization of the error in (46) has been accomplished, then the phase estimate is found as

$$\tilde{\theta} = \theta + \beta n_t \tag{47}$$

where n_t is the waveform index value at the height track point. The minimization is very rapid because near convergence the derivatives of the error are nearly linear in θ and β where the waveform SNR ratio is significant.

In addition to removing the impact of slope in the cross-channel waveform phase, the above procedure performs a weighted averaging of several waveform values to produce the final phase estimate. For the case of a surface slope of 0.3°, 1000 simulations each involving the averaging of 100 waveforms have been performed in which waveform samples

TABLE III
SIMULATED ELEVATION MEASUREMENT PRECISION FOR A FLAT SURFACE TILTED BY 0.3° RELATIVE TO THE ANTENNA DISPLACEMENT AND THE ANTENNA BORESIGHT. THE ANGLE ESTIMATION IS MADE FROM EIGHT WAVEFORM SAMPLES ON EITHER SIDE OF THE WAVEFORM LEADING EDGE. EACH VALUE IS THE RESULT OF 1000 SIMULATIONS EACH INVOLVING THE AVERAGING OF 100 ALTIMETER WAVEFORMS. THE PREDICTED PRECISION DOES NOT INCLUDE THE IMPACT OF AVERAGING WAVEFORM SAMPLES. THE SYSTEM AND GEOMETRY PARAMETERS ARE GIVEN IN TABLE I

SNR (dB)	Simulated Precision (cm) flat surface	Prediced Precision (cm) flat surface	1-m rms roughness	2-m rms roughness
10	1.89	2.60	2.77	3.02
15	0.69	0.87	1.01	1.23
20	0.30	0.34	0.48	0.69
25	0.17	0.18	0.32	0.52
30	0.12	0.13	0.26	0.47

24–40 have been used to estimate the slope in the phase and determine the angle estimate. The first point on the plateau of the waveform is sample 32 so the phase determination is based on eight samples before and eight samples after the waveform leading edge. The resulting phase angle and surface elevation precision for SNR's of 10, 15, 20, 25, and 30 dB are shown in Table III. The elevation precision in that table, while involving the complication of estimating the phase slope, are better than those values shown in Fig. 7 for the level surface. In the latter case, only one waveform sample was used. These values are also shown in Table III for comparison. It is seen in these results that using several waveform points in the angle measurement improves the precision for low SNR's but results in little change for high SNR's. This is a result of the weighting in (46) which emphasizes a single, highly coherent point at the waveform leading edge for high SNR while allowing for an averaging of several points where the coherence is limited by thermal noise and is roughly constant across several waveform samples.

The elevation errors listed in Table III show that even in the presence of a surface slope, an elevation precision better than 1 cm can be achieved with reasonable system parameters. Of course, we have focused exclusively on the instrument angle measurement precision here and other sources of error, such as satellite attitude determination and range measurement precision will contribute to the overall system performance. Nonetheless, this analysis shows that the statistical nature of the angle measurement will support the required elevation precision.

B. Impact of Scattering Surface Roughness

All of the analytical and simulation work presented here pertains to the case of a flat surface. The surface has been tilted, but no surface roughness has been considered. The impact of roughness will be to increase the size of the measurement area and reduce the coherence of the surface scattered pulse [2]. Surface roughness will result in an effective pulse width that is the root-sum-of-squares of the actual pulse

width and the root mean square (rms) surface roughness. That is

$$\Delta_{\text{eff}} = \sqrt{\Delta^2 + h^2} \tag{48}$$

where Δ_{eff} is the effective range resolution and h is the rms value of the surface roughness.

A 1-m rms roughness will increase the effective pulse width from about 0.47 m to about 1.10 m. The elevation precision will degrade proportionately. The rightmost two columns of Table III shows the predicted elevation precision as a function of both the SNR and the rms surface roughness for the parameters shown in Table I.

C. Impact of Volume Scattering

The analysis presented above is based on a consideration of surface scattering only. Volume scattering plays an important role in altimetry of the ice [15]. While a full treatment of volume scattering is beyond the scope of this paper, volume scattering will not reduce the utility of a radar altimeter for the observation of changes in the ice elevation so long as two assumptions are made: that the extent of volume scattering is uniform over the illuminated area and that the volume scattering remains constant between elevation measurements. The angle measurement will not be reduced by volume scattering because it will not result in a decorrelation of the signal in the two receiver channels. The measured elevation will be beneath the elevation of the physical surface, but this will not be a problem for observations of elevation change. Recovery of the surface elevation from the altimeter waveform, such as has been done with conventional altimetry [15], may be applied with equal success in conjunction with the angle measurement. Further work will be required to fully assess this and other issues involved in specific applications of the angle measurement performed by a phase monopulse radar altimeter.

V. Conclusions

The measurement of angle with a radar altimeter through phase comparison monopulse techniques can be done with a precision that will support centimeter scale elevation measurements even when the measurement is made over a tilted surface. The elevation precision is independent of the tilt angle so long as the measurement area remains within the transmit/receive antenna beamwidth. This precision can be supported for both the annular and linear measurement areas as demonstrated by both analysis and simulation.

The elevation errors resulting from angle measurement errors within the altimeter itself will be combined with errors in the spacecraft attitude knowledge and errors in the range measurement. If the attitude error is 0.01°, then this will contribute about 1.2 cm to the elevation error, as defined by (5). Together, the angle measurement and attitude knowledge at this level will contribute less than 2 cm to the total system performance. Such an approach, therefore, will support high-resolution altimetry over tilting surfaces such as the polar ice sheets.

Acknowledgment

The author would like to thank Prof. R. Joseph for assistance in determining the probability density function for the phase of the measured angle.

References

[1] G. S. Brown, "The average impulse response of a rough surface and its applications," *IEEE Trans. Antennas Propagat.*, vol. AP-25, pp. 67–74, 1977.
[2] D. B. Clelton, E. J. Walsh, and J. L. MacArthur, "Pulse compression and sea level tracking in satellite altimetry," *J. Atmospheric Oceanic Tech.*, vol. 6, no. 3, pp. 407–438, June 1989.
[3] H. J. Zwally, "Growth of Greenland ice sheet: Interpretation," *Science*, vol. 246, pp. 1589–1591, 1989.
[4] R. Warrick and J. Oerlemans, "Sea level rise," in *Climate Change, The IPCC Scientific Assessment.* Cambridge, U.K.: Cambridge Univ. Press, 1990, pp. 261–281.
[5] J. Oerlemans, "Possible changes in the mass balance of the Greenland and Antarctic ice sheets and their effects on sea level," in *Climate and Sea Level Change.* Cambridge, U.K.: Cambridge Univ. Press, 1993, pp. 144–161.
[6] D. J. Wingham, C. G. Rapley, and J. G. Moreley, "Improved resolution ice sheet mapping with satellite radar altimeters," *EOS*, vol. 74, no. 10, pp. 113, 116.
[7] H. J. Zwally, J. A. Major, A. C. Brenner, and R. A. Binschadler, "Ice measurements by Geosat radar altimeter," *Johns Hopkins APL Tech. Dig.*, vol. 8, no. 2, pp. 251–254.
[8] C. J. Choe and B. E. Schutz, "Estimation of ice sheet surface elevation change from the EOS laser altimeter satellite (ICESAT) crossover simulations," *Advances Astronautical Sci.*, vol. 93, pp. 1623–1635, 1996.
[9] J. R. Jensen and R. K. Raney, "Multimission radar altimeter: Concept and performance," in *Proc. Int. Geosci. Remote Sensing Symp. IGARSS'96*, Lincoln, NE, May 1996, pp. 2279–2281.
[10] R. K. Raney, "The delay/Doppler radar altimeter," *IEEE Trans. Geosci. Remote Sensing*, vol 36, pp. 1578– 1588, Sept. 1998.
[11] P. C. Marth *et al.*, "Prelaunch performance of the NASA altimeter for the Topex/Poseidon project," *IEEE Trans. Geosci. Remote Sensing*, vol. 31, pp. 315–332, Mar. 1993.
[12] C. R. Valverde, R. K. Stilwell, A. A. Russo, and T. R. McKnight, "The S-band beacon receiver for the midcourse space experiment," *Johns Hopkins APL Tech. Dig.*, vol. 15, no. 1, Jan. 1994.
[13] M. Abramowitz and I. Stegan, *Handbook of Mathematical Functions.* New York: Dover, 1965.
[14] D. Middleton, *An Introduction to Statistical Communication Theory.* Los Altos, CA: Peninsula, 1987.
[15] C. H. Davis and R. K. Moore, "A combined surface and volume scattering model for ice-sheet radar altimetry," *J. Glaciology*, vol. 39, pp. 675–686, 1993.

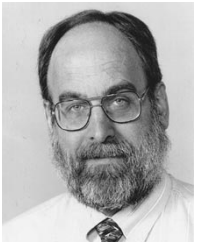

J. Robert Jensen (M'92) received the B.A. degree from Cornell College, Mt. Vernon, IA, in 1973 and the Ph.D. degree in physical chemistry from the University of Wisconsin, Madison, in 1978.

He joined the Applied Physics Laboratory of the Johns Hopkins University in 1978 and worked on a variety of nonacoustic detection problems, principally involving radar performance analysis, signal processing algorithms, and rough surface scattering. In 1989 he joined the APL Space Department and has participated in the TOPEX altimeter preflight testing, the development and testing of algorithms for the beacon receiver on the MSX Satellite, the NEAR telecommunications systems, and on other satellite programs including the Geosat Follow-on Program for which APL was the Navy's technical direction agent.

Dr. Jensen is a member of the APL Principal Professional Staff and the AGU.